Supplementary Information

Bionanocomposite Hydrogel for the Adsorption of Dye and Reusability of Generated Waste for the Photo-degradation of Ciprofloxacin: A Demonstration of the Circularity Concept for Water Purification

Neeraj Kumar[a*], Hemant Mittal[b], Saeed M. Alhassan[b], Suprakas Sinha Ray[a,c*]

[a]*DST-CSIR National Centre for Nanostructured Materials, Council for Scientific and Industrial Research, Pretoria 0001, South Africa*
[b]*Department of Chemical Engineering, Khalifa University of Science and Technology, PO Box 2533, Abu Dhabi, United Arab Emirates*
[c]*Department of Applied Chemistry, University of Johannesburg, Doornfontein 2028, South Africa*

*Corresponding authors: N. Kumar (nkumar@csir.co.za; ynk.neeraj@gmail.com), and S. S. Ray (rsuprakas@csir.co.za; ssinharay@uj.ac.za)

Contents

Characterization techniques used

The X-ray diffraction patterns of initially and after used hydrogel were executed using PANalytical X' Pert Pro diffractometer with X-ray source of Cu Kα radiation (λ = 1.5406 Å) at operation voltage and current of 45 kV and 40 mA respectively. Field Emission-Scanning Electron Microscope (Auriga FESEM, Carl Zeiss, Germany) with coupled with an Oxford energy dispersive X-ray spectrometer (EDS, Oxford, UK) was used to realize the surface morphologies changes in fresh and applied nanocomposite hydrogel. The distribution of TiO_2 NRs within the hydrogel was investigated using a High Resolution Transmission Scanning Electron Microscope (HR-TEM; STEM, JEOL, 2100-JEM Japan) at an operating voltage of 200 kV coupled with an EDS (Thermo Scientific, USA). An Attenuated Total Reflectance-Fourier Transform Infrared (ATR-FTIR, Spectrum 100, Perkin-Elmer, USA) was used to obtain FTIR spectra in a dispersive mode in the range of 550-4000 cm^{-1} at a resolution of 4 cm^{-1}/s. X-ray Photoelectron Spectroscopy (XPS) data was collected to check the binding energy of elements of TGB hydrogel and photocatalyst using Kratos Axis Ultra device (Kratos, UK) using monochromatic Al Kα excitation radiation. Nitrogen adsorption/desorption isotherms were determined using Micromeritics (ASAP 2020, USA) surface area analyzer and Multi-Point Brunauer–Emmett–Teller (BET) analysis was carried out to find out specific surface area. UV-Vis measurements were carried out on LAMBDA 750 UV/Vis/NIR Spectrophotometer, PerkinElmer, USA. A Horiba Jobin-Yvon NanoLog spectrometer, USA with 450 W xenon short-arc as excitation source was used to measure photoluminescence spectra. Thermogravimetric analysis (TGA) of prepared hydrogel was acquired using TGA Q500, USA in N_2 gas atmosphere with a heating rate of 10 °C/min. Raman measurements were achieved using Horiba Scientific, USA with using green laser light (515 nm). Mott-Schottky plots were received using three-electrode cell electrochemical workstation (SP-200 Potentiostat Biologic Science Instruments). The data were obtained at a fixed frequency of 1 kHz in a 0.5 M KOH solution.

Procedure for the adsorption studies

In the present study, a cationic triarylmethane dye, namely brilliant green (BG), was chosen as the modal pollutant for investigating the adsorption performance of the as-prepared TGB-hydrogel. A batch adsorption method was employed to elucidate the adsorption characteristics of BG from aqueous solutions. The required concentration of dye solution was obtained by simply diluting the stock solution with deionized water. In the adsorption experiment, a preweighed sample of the TGB-hydrogel was added to 100 mL of a predetermined modal dye solution and agitated in a thermostatic incubator shaker (Separation Scientific, SA) at 250 rpm for 24 h. The adsorption temperature was kept constant at 25 ± 0.2 °C (unless otherwise noted), and the pH of the solution was adjusted and maintained at the target level during the course of the experiment with 0.1 M HCl or NaOH. After completion of the experiment, an aliquot was removed from the solution and filtered through a 0.45-μm membrane filter. The concentration of the supernatant was subsequently determined by UV-vis spectrophotometry at the absorbance maximum for BG (λ_{max} = 625 nm) aided by a calibration curve. For the kinetics experiments, the required amount of hydrogel was added to dye solutions of varying concentration for fixed periods of time. Numerous solution samples were prepared for each dye concentration, and a single sample was used for each time interval. The adsorption capacity at time t (q_t), adsorption capacity at equilibrium (q_e), and BG-removal efficiency by the TGB-hydrogel were determined using eqns. 2–4.

$$Percentage\ removal = \frac{C_o - C_e}{C_o} \times 100 \qquad (1),$$

$$q_e\ (\mathrm{mg/g}) = \frac{C_o - C_e}{m} \times V \qquad (2),$$

$$q_t\ (\mathrm{mg/g}) = \frac{C_o\ -\ C_t}{m} \times V \qquad (3),$$

where C_0 and C_e (mg/L) are the initial and equilibrium concentrations of the dye solution, respectively, m (g) is the subjected mass of the hydrogel, and V (L) is the removed volume of the dye solution. In order to determine the best performance conditions, the adsorption characteristics of the as-synthesized TGB-hydrogel were investigated against various adsorbent dosages (0.01-0.10 g), pH (2.0–11.0), dye-solution

temperatures (303, 313, and 323 K), initial dye concentrations (100–600 mg L^{-1}), regeneration, and recyclability. TGB-hydrogel reusability was examined in ethanol over five consecutive adsorption-desorption cycles.

Photocatalytic performance of the C-TiO_2 NC

The material obtained following adsorption studies was washed thoroughly with deionized water, thermally activated (calcined at 550 °C for 3h), and reused for the photocatalytic degradation of CIP. Herein, 40 mg of the waste-derived TGB-hydrogel was added to a solution of CIP (15 mgL^{-1}) and stirred at 300 rpm at 25 ± 2 °C. The pH of the CIP solution was controlled by the addition of 0.1 M NaOH or HCl in order to determine optimum photocatalytic efficiency. A UV-vis light system (medium-pressure Hg lamp, 250 W) was used to irradiate the CIP solution in a dark chamber. The distance between the CIP solution and light source was adjusted to be 5 cm. Before illumination, the CIP solution containing the photocatalyst was magnetically stirred (300 rpm) and left in the dark for 30 min to establish adsorption-desorption equilibrium between the CIP molecules and the photocatalyst. A 3-mL aliquot of the CIP solution was collected for analysis and centrifuged to remove suspended photocatalyst particles. Absorption spectra were acquired in order to monitor the degradation rate by following the absorption intensity at the wavelength maximum of CIP (λ_{max} = 275 nm) using a UV-vis spectrophotometer. Furthermore, the effects of sacrificial agents, such as isopropyl alcohol (IPA), disodium ethylenediaminetetraacetate (EDTA-2Na), and benzoquinone (BZQ), on photocatalytic efficiency were examined. A blank test was also performed using the optimized conditions in the absence of the photocatalyst. For recycling experiment, C-TiO_2 NC photocatalyst was washed using deionized water and dried in air oven and then used for next cycle.

Table 1: Illustrates the varied concentration of TiO_2 in hydrogel and swelling capacity.

Hydrogel	**Amount of TiO_2 (mg)**	**P_s**
Polymer matrix	-	1395.71
TGB1-hydrogel	15	1613.42
TGB2-hydrogel	25	1801.56
TGB3-hydrogel	35	2289.92
TGB4-hydrogel	45	2124.38
TGB5-hydrogel	55	1907.05

Scheme 1. Plausible synthesis mechanism for the grafting of Gg using poly(acrylamide-co-acrylic acid) and formation of TGB-hydrogel: (i) initiation; (ii) grafting copolymerization, (iii) crosslinking, (iv) incorporation of TiO_2 NRs onto hydrogel polymer matrix to form TGB-hydrogel.

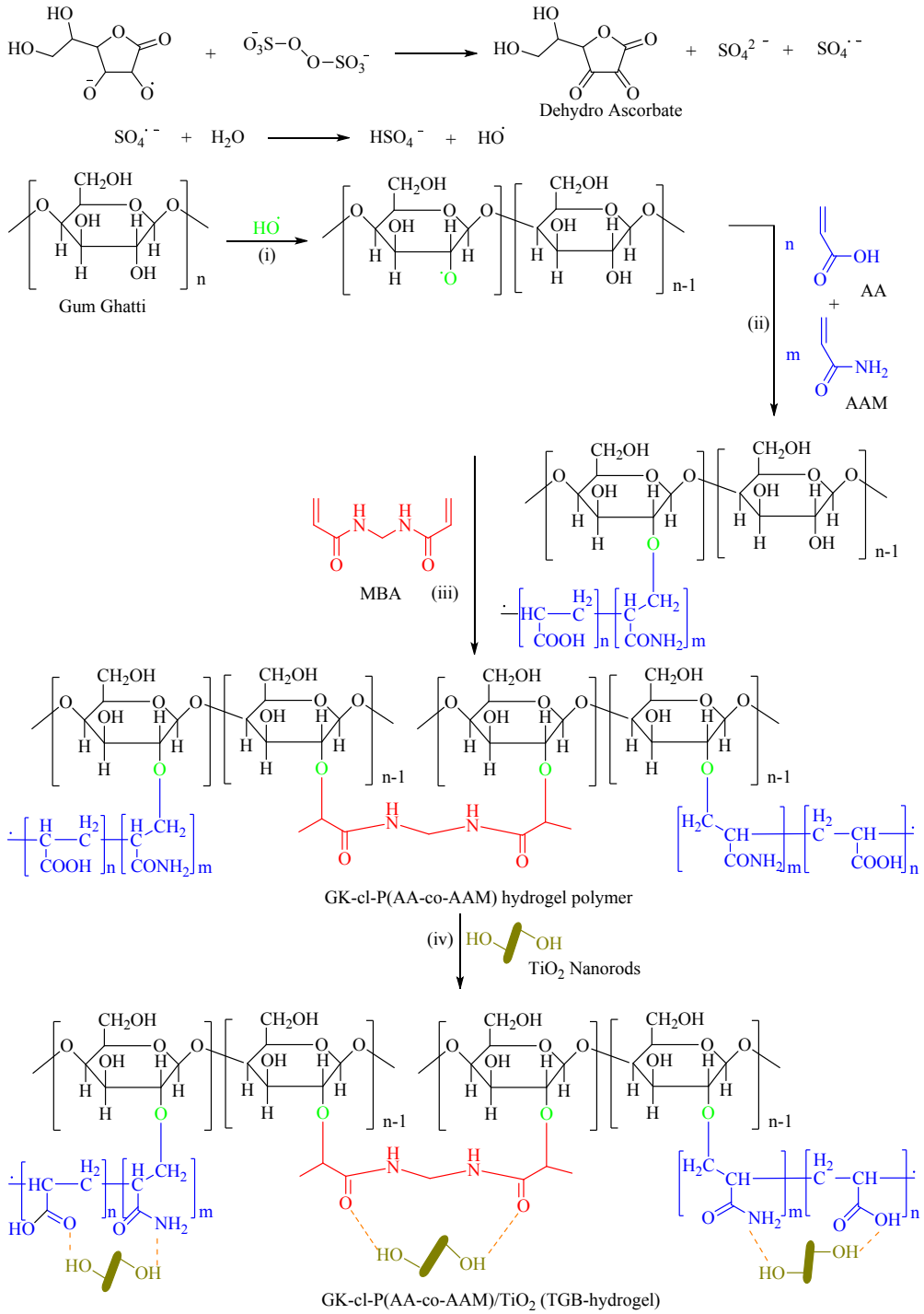

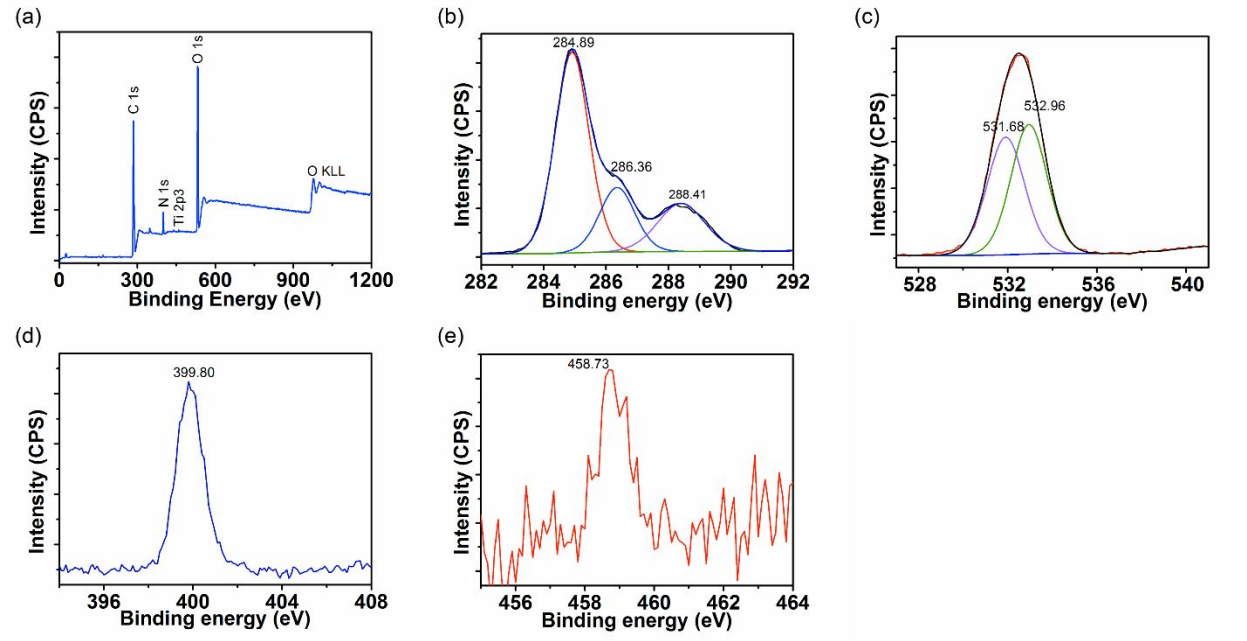

Fig. S1 XPS survey spectrum of (a) TGB-hydrogel and high resolution spectra of (b) C 1s, (c) O 1s, (d) N 1s, and (e) Ti 2p3.

Table S2: Different kinetics models used in the present study

Name	**Expression**	**Eq. no**	**Parameters**
Pseudo-first-order	$q_t = q_e(1 - e^{-k_1 t})$	(S4)	k_1: Pseudo first order rate constant, min-1
Pseudo-second-order	$q_t = \frac{k_2 {q_e}^2 t}{1 + k_2 q_e t}$	(S5)	k_2: Pseudo second order rate constant, g.mg^{-1}.min^{-1}
Elovich	$q_t = \frac{1}{\beta}\ln(\alpha\beta) + \frac{1}{\beta} lnt$	(S6)	α : Initial adsorption rate constant, mg.g.$^{-1}$.min^{-1} β: Adsorption rate constant during any one experiment, g.min^{-1}
Intraparticle diffusion	$q_t = k_{ID} t^{\frac{1}{2}} + C$	(S7)	k_{ID}: Intraparticle diffusion rate constant, mg g^{-1}.min$^{-1/2}$ C: Intercept, mg.g^{-1}
Liquid film diffusion	$ln\left(1 - \frac{q_t}{q_e}\right) = C_1 - k_{FD} t$	(S8)	k_{FD}: Diffusion rate constant, min^{-1} C_1: Constant

Table S3: List of the adsorption isotherm models used in this study

Model	Equations	Eq. No.	Parameters
Two-parameter models			
Langmuir	$q_e = \frac{q_m K_L C_e}{1 + K_L C_e}$ $R_L = \frac{1}{1 + K_L C_O}$	(S9) (S10)	qm: Maximum capacity of adsorption, mg g^{-1} K_L: Affinity of the binding sites, L mg^{-1} R_L: Separation factor
Freundlich	$q_e = K_F C_e^{\frac{1}{n}}$	(S11)	K_F: Freundlich parameter, (L mg^{-1})$^{1/n}$(mg g^{-1}) n: Heterogeneity parameter (n<1)
Temkin	$q_e = B ln(K_T C_e)$ $B = \frac{RT}{b_T}$	(S12) (S13)	B: Temkin Parameter, mg g^{-1} K_T: Adsorption capacity, L mg^{-1} b: Heat of sorption, kJ mol^{-1}
Dubinin-Radushkevich	$q_e = q_m \exp(-K_{DR}\varepsilon^2)$ $\varepsilon = RT ln\left(1 + \frac{1}{C_e}\right)$ $E_s = \frac{1}{(2\beta)^{1/2}}$	(S14) (S15) (S16)	q_m: Maximum capacity of adsorption, mg g^{-1} ε: Polanyi potential K_{DR}: DR constant, mol^2 J^{-2} E_S: Free energy of sorption per mole of the adsorbate, kJ mol^{-1}
Jovanovic	$q_e = q_m[1 - \exp(-K_J C_e)]$	(S17)	q_m: Maximum capacity of adsorption, mg g^{-1} K_J: Jovanovic's parameter, L mg^{-1}
Halsey	$q_e = \exp\left[\frac{lnK_H + lnC_e}{n}\right]$	(S18)	K_H: Halsey's parameter, L mg^{-1} n: Halsey's Exponent

Table S4: The evaluated fitted parameters along with the related error values for each individual adsorption isotherm models

Isotherm models	Parameters	Temperature (°C)		
		30	**40**	**50**
Two parameter models				
Langmuir	q_m (mg.g^{-1})	740.97	773.68	817.63
	K_L (L.mg^{-1})	6.59x10^{-2}	6.79x10^{-2}	7.80x10^{-2}
	R_L	0.024-0.215	0.024-0.210	0.020-0.188
	Reduced χ^2	25.010	34.277	38.147
	RSS	250.10	342.77	381.47
	R^2	0.999	0.999	0.999
Freundlich	K_F (L.mg^{-1})1/n(mg.g^{-1})	174.41	180.61	200.517
	1/n	0.263	0.267	0.261
	Reduced χ^2	4600.27	5214.79	6661.75
	RSS	46.0x10^2	52.14 x10^2	66.61x10^2
	R^2	0.891	0.890	0.879
Temkin	β (mg.g^{-1})	18.44	17.535	16.858
	K_T (L.mg^{-1})	0.963	0.967	1.160
	Reduced χ^2	1313.07	1418.314	1987.84
	RSS	13.13x10^2	14.18x10^2	19.87x10^2
	R^2	0.969	0.976	0.967
DKR	q_D (mg.g^{-1})	630.73	656.76	699.63
	K_{DR} (mol^2.J^{-2})	1.130x10^{-5}	1.036x10^{-5}	9.02x10^{-6}
	E_s (kJ.mol^{-1})	2.10	2.91	2.35
	Reduced χ^2	6583.40	6938.87	7648.89
	RSS	65.83x10^2	69.38x10^2	76.48x10^2
	R^2	0.846	0.854	0.861
Jovanovic	q_m (mg.g^{-1})	666.49	694.41	736.71
	K_J (L.mg^{-1})	5.19x10^{-2}	5.39x10^{-2}	6.17x10^{-2}
	Reduced χ^2	958.67	1095.75	929.36
	RSS	95.86x10^2	10.95x10^2	92.93x10^2
	R^2	0.977	0.977	0.983
	K_H (mg.g^{-1})	3.25x10^8	2.82x10^8	6.35x10^8

Halsey				
	n	3.797	3.744	3.817
	Reduced χ^2	4660.27	5214.79	6661.75
	RSS	46.60×10^2	52.14×10^2	66.61×10^2
	R^2	0.891	0.890	0.879

The maximum adsorption capacities (q_m) determined by Langmuir isotherm model and mean adsorption capacity (q_D) determined using DKR model vary greatly due to consideration of different assumptions during formulation of these isotherms. In Freundlich isotherm, the reciprocal of heterogeneity factor (1/n) were found to be less than one, depicts the adsorption was satisfactory for a whole range of dye concentrations. The Temkin isotherm, the value of β increased with increasing temperature, supports the endothermic nature of adsorption.

Table S5. Equations needed for calculation of thermodynamic parameters.

Calculations	**Equations**	**Eq. No.**	**Parameters**
Van't Hoff graph	$\ln K_L = \frac{\Delta S°}{R} + \frac{-\Delta H°}{RT}$	(S19)	$\Delta H°$: Change in enthalpy (J/mol), $\Delta S°$: Change in entropy (J/mol.K), T : Absolute temperature (K), R : universal gas constant (8.314 J/K.mol).
Free energy	$\Delta G° = -RT ln K_L$	(S20)	$\Delta G°$: change in Gibbs free energy (J/mol)
K_L	$K_L = m\frac{q_e}{C_e}$	(S21)	K_L is the distribution coefficient

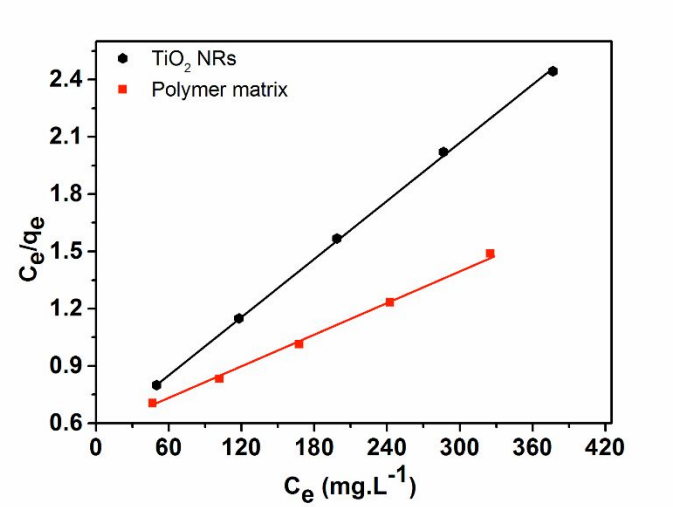

Fig. S2. Comparison of the adsorption capacity of TiO_2 NRs and polymer matrix.

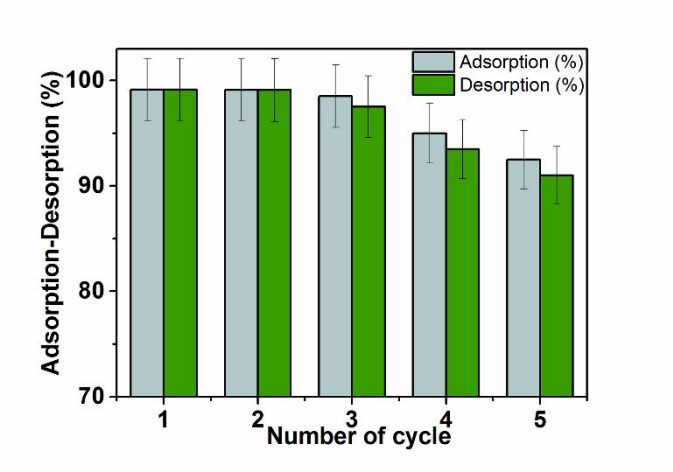

Fig. S3. Adsorption-desorption efficiency of the TGB-hydrogel in multiple cycles of regeneration

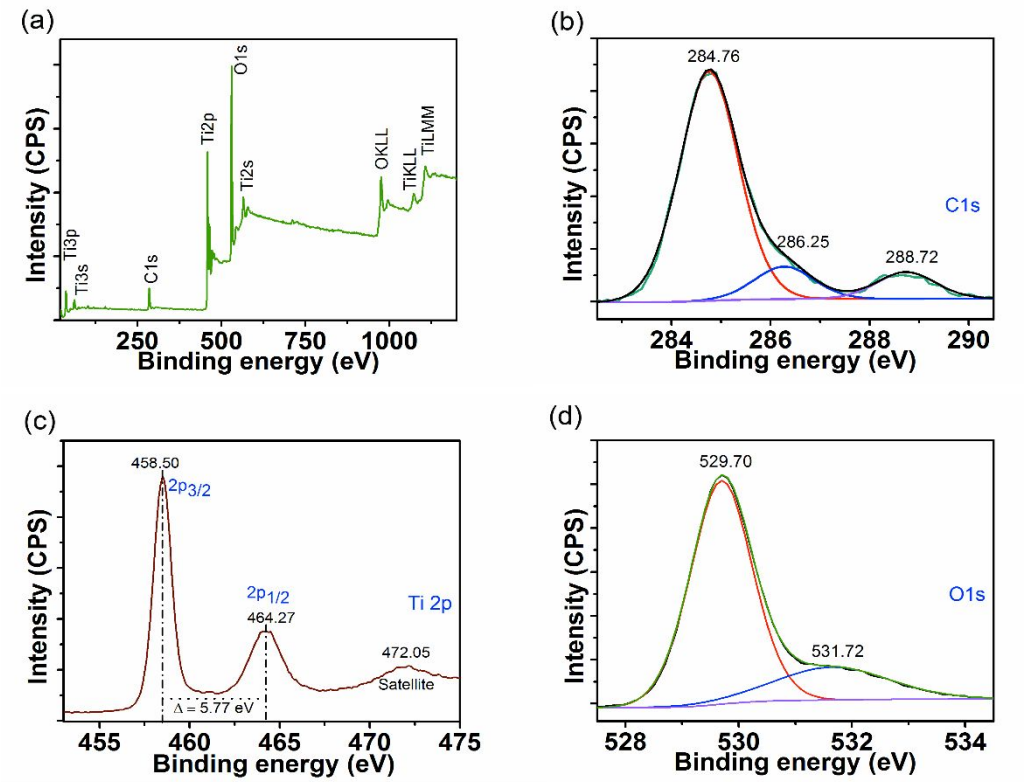

Fig. S4 XPS survey spectrum of (a) C-TiO_2 NC and high resolution spectrum of (b) C1s, (c) Ti2p, (d) O1s

The XPS survey spectrum clearly showed the typical peaks of C, O, and Ti elements (**Fig. S3**). The high resolution spectrum of C1s exhibited the three peaks centered at 284.76, 286.25 and 288.72 eV could be attributed to –C-C/-C=C/-C-H, -C-OH/C-O-C/C-N and –COOH, respectively. The high-intensity peak at 284.76 eV might be related to the large amount of –C-C/C=C/C-H networks. However, in the case of Ti 2p spectrum, the first unsymmetrical peak with maxima at 458.50 eV could be attributed to TiO_2 (Ti^{4+}) and Ti_2O_3 (Ti^{3+}) in $Ti2p_{1/2}$ (lower value) and $Ti2p_{3/2}$ (higher value), respectively. The line separation energy between $Ti2p_{3/2}$ and $Ti2p_{1/2}$ was 5.77 eV, which was consonant with TiO_2 standard binding energy[1-2]. The satellite peak at 472.05 possibly occurred due to the interaction of outgoing electron with valence electron which in turn excited to higher energy level[2]. The O1s spectrum was deconvoluted into two Gaussian components at 529.70 and 531.72 eV. The peaks at 529.70 eV could be accredited to oxygen associated to the Ti^{4+} in TiO_2. The shoulder at 530.7 eV implied that the surface was partially covered with the –OH/–

O-C groups[3]. This observation further supports the existence of oxygen vacancies, which would introduce the number of defects in C-TiO_2 NC. The binding energy at 531.72 eV was ascribed to >C=O groups or absorbed oxygen.

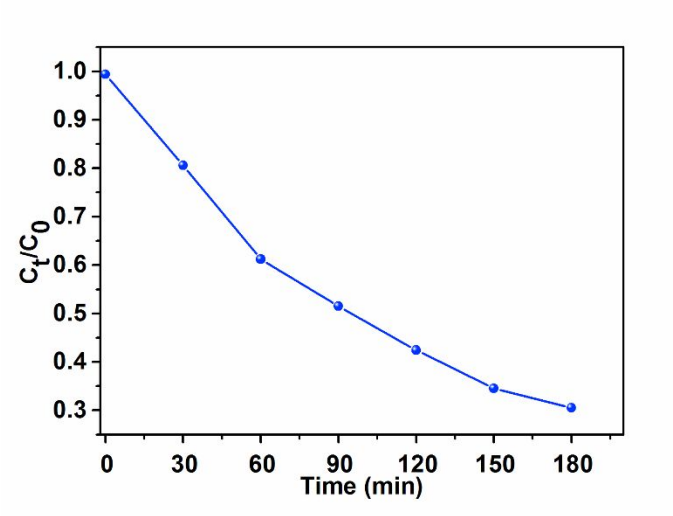

Fig. S5 Photocatalytic efficiency of bare TiO_2 NRs for CIP degradation

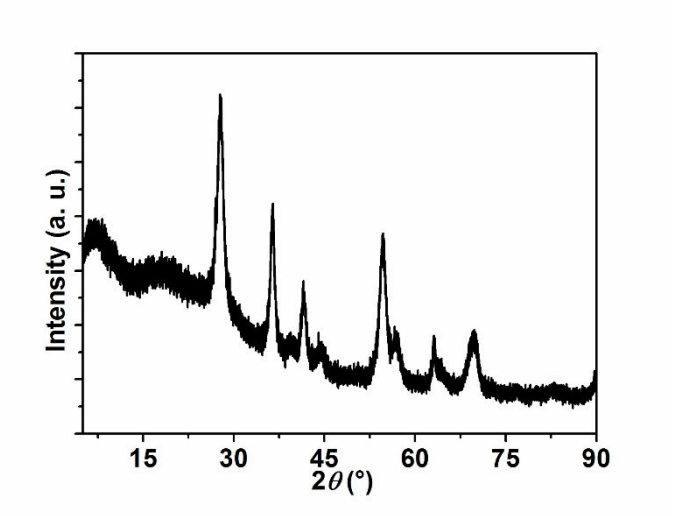

Fig. S6 XRD pattern of spent C-TiO_2 NC obtained after photocatalytic degradation of CIP

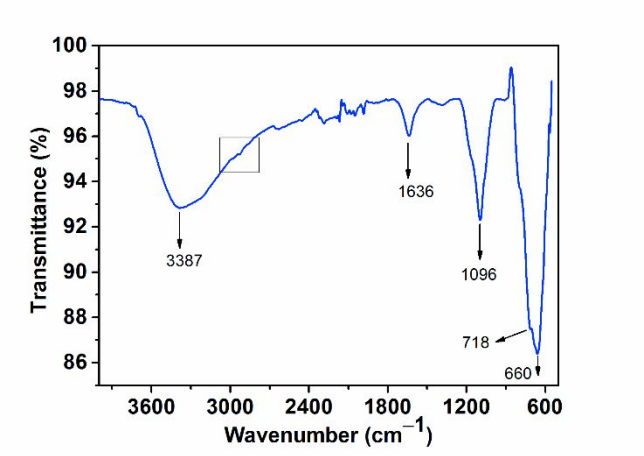

Fig. S7 FTIR spectrum of spent C-TiO_2 NC obtained after photocatalytic degradation of CIP

Reference

1. Ma, L.; Huang, Y.; Hou, M.; Xie, Z.; Zhang, Z., Ag Nanorods Coated with Ultrathin TiO2 Shells as Stable and Recyclable SERS Substrates. *Scientific Reports* **2015,** *5*, 15442.

2. Jia, L.; Xie, J.; Guo, C.; Li, C. M., Modification of a thin layer of α-Fe2O3 onto a largely voided TiO2 nanorod array as a photoanode to significantly improve the photoelectrochemical performance toward water oxidation. *RSC Advances* **2015,** *5* (77), 62611-62618.

3. Jackman, M. J.; Thomas, A. G.; Muryn, C., Photoelectron Spectroscopy Study of Stoichiometric and Reduced Anatase TiO2(101) Surfaces: The Effect of Subsurface Defects on Water Adsorption at Near-Ambient Pressures. *The Journal of Physical Chemistry C* **2015,** *119* (24), 13682-13690.